Tellus (1996), 48A, 403–423
Printed in UK – all rights reserved



TELLUS
ISSN 0280–6495

# The effect of vertical resolution on clear-sky radiation calculations: tests with two schemes

By PETRI RÄISÄNEN*, *Department of Meteorology, P.O. Box 4, SF-00014 University of Helsinki, Finland*

(Manuscript received 16 June 1995; in final form 28 September 1995)

ABSTRACT

The dependence on vertical resolution of the clear-sky results produced by two radiation codes (a slightly modified version of the ECMWF scheme and the scheme used at the DWD) is investigated. Results are presented both for the McClatchey et al. atmospheres and for a set of fully detailed sounding profiles measured at Jokioinen, Finland. The effect of vertical discretization on shortwave calculations is found to be very small, particularly for the DWD scheme. The downward longwave flux at the surface is found to be sensitive to vertical resolution only in the lower troposphere, whereas for the upward flux at the top of the atmosphere, upper tropospheric resolution seems the most important. The major difference found between the smooth McClatchey et al. profiles and the detailed soundings is that discretization errors of longwave cooling rates are larger for the latter data set, particularly in the lower troposphere. Furthermore, in cases with sharp surface inversions, large errors of downward longwave flux at the surface occur if there is poor resolution in the boundary layer. The average errors of the longwave fluxes at the boundaries are, however, fairly similar for the two data sets. Quantitatively, the discretization errors of longwave fluxes are relatively small, especially for the ECMWF scheme. About 20 layers is sufficient for both schemes to keep the maximum value of net flux error in the vertical column within 2 $Wm^{-2}$ even for most of the detailed sounding profiles. For the calculation of radiative fluxes, it seems preferable to have the majority of the layers in the troposphere. Finally, the profiles of longwave fluxes and cooling rates in surface inversion situations are discussed.

## 1. Introduction

The fundamental rôle that radiative processes play in forming the climate of the Earth makes accurate radiation calculations vitally important for numerical climate modelling. Yet, in practice, various factors cause inaccuracy in the radiation schemes. A major effort to evaluate the magnitude of the differences between the radiation code results, and to understand the causes leading to these differences, has been made in the Intercomparison of Radiation Codes Used in Climate Models (ICRCCM) project (Ellingson et al., 1991; Fouquart et al., 1991).

In this paper, one particular problem related to radiation parameterization is addressed: the sensitivity of the results to vertical discretization, that is, the number and location of layers in the atmospheric model. A few notes on this subject, concerning clear-sky longwave calculations, have already appeared in the meteorological literature. Rodgers and Walshaw (1966), testing a narrow-band model for rather smooth sounding profiles, found differences in cooling rates of only 0.01–0.03 K/d when changing from a grid with 25 layers to one with 13 layers. Morcrette and Fouquart (1985), testing their narrow-band model for the

E-mail: Petri.Raisanen@Helsinki.Fi

McClatchey et al. (1971) standard atmospheres, end up with a somewhat more pessimistic estimate. They conclude that given their vertical integration method, about 40 layers, 20 in the troposphere and 20 in the stratosphere, would be needed to get a proper representation of radiative fluxes at the surface, at the tropopause level, and at the top of the atmosphere, and to keep errors in total atmospheric longwave divergence within 2 $\mathrm{Wm}^{-2}$. They also found that layers with equal pressure thickness gave a good presentation of cooling rates in the troposphere, whereas in the stratosphere, it was preferable to keep the change in the logarithm of pressure across layers approximately constant. In addition, comparison of numerical quadratures (2- or 8-point gaussian quadrature, trapezoidal rule) is reported in their paper. The differences between different numerical integration techniques are also addressed in Ridgway et al. (1991), in the context of longwave cooling rates calculated with a line-by-line model.

An obvious, though important fact, is that the effects of vertical discretization are model-dependent. The usefulness of testing the resolution dependence of the results is highlighted by the findings of Ellingson et al. (1991): in the ICRCCM comparison, unsatisfactory methods for performing the integration over altitude were identified as one of the major error sources in clear-sky longwave calculations. Thus, in some radiation schemes, the sensitivity to vertical resolution may be substantially larger than the studies cited above suggest.

In this study, the resolution sensitivity of two radiation schemes is described. One of the schemes tested was the European Centre for Medium Range Weather Forecasts (ECMWF) radiation code (Morcrette, 1989, 1991), the other one was the scheme designed by Ritter and Geleyn (1992) and used at the Deutscher Wetterdienst (DWD). In the following, the schemes will be referred to with the names of their host models. Both schemes are detailed, state-of-the-art wide-band models. However, the details of the parameterization of gas absorption differ a lot from one scheme to another, and, in particular, the basic approach used to solve the radiative transfer equation in the longwave region is different. Thus, the schemes are quite independent, which makes a comparison of their behaviour interesting.

As in the above-mentioned studies, the emphasis is on clear-sky longwave calculations. However, two aspects of the problem are handled more carefully than has been done before. First, the relative importance of resolution in different parts of the atmosphere is addressed more systematically. Second, results are presented also for a set of very detailed sounding profiles.

## 2. The radiation codes

The vertical discretization experiments were performed with a slightly modified version (see below) of the ECMWF cycle 45 radiation scheme and the version of the DWD scheme operational in late 1993. Here, only the aspects of the schemes most relevant to the vertical discretization studies are described. A more thorough description of the ECMWF and DWD radiation schemes can be found in Morcrette (1989, 1991) and Ritter and Geleyn (1992), respectively.

In the ECMWF radiation code, the shortwave (solar) and longwave (terrestrial) parts of the spectrum are divided into 2 and 6 intervals, respectively; the corresponding split in the DWD scheme is 3 and 5. In the shortwave calculations, both schemes make use of a delta-two-stream approach, the details of which differ slightly. In the longwave calculations, however, there is a more profound difference between the schemes.

In the ECMWF scheme, the "τdB-formulation" of the so-called emissivity-type method is used in the longwave calculations. This method is based on the integral solution of the radiative transfer equation in a non-scattering medium. For each spectral interval, the radiative fluxes at a pressure level $p$ are calculated from the equations

$$F^{\uparrow}_{\Delta\nu}(p) = [(1-\varepsilon_{g\Delta\nu})F^{\downarrow}_{\Delta\nu}(p_s) + \varepsilon_{g\Delta\nu}B_{\Delta\nu}(T_s) - B_{\Delta\nu}(T_{0+})]\tau^{f}_{\Delta\nu}(p, p_s) + B_{\Delta\nu}(T_p) + \int_{p}^{p_s} \tau^{f}_{\Delta\nu}(p, p') \frac{\mathrm{d}B_{\Delta\nu}(T_{p'})}{\mathrm{d}p'}\,\mathrm{d}p', \quad (1)$$

$$F^{\downarrow}_{\Delta\nu}(p) = -B_{\Delta\nu}(T_\infty)\tau^{f}_{\Delta\nu}(p,0) + B_{\Delta\nu}(T_p) + \int_{p}^{0} \tau^{f}_{\Delta\nu}(p, p') \frac{\mathrm{d}B_{\Delta\nu}(T_{p'})}{\mathrm{d}p'}\,\mathrm{d}p', \quad (2)$$

where $F^{\uparrow}_{\Delta\nu}$ and $F^{\downarrow}_{\Delta\nu}$ denote upward and downward fluxes integrated over the spectral interval $\Delta\nu$, $B_{\Delta\nu}$ is the Planck function, $p_s$ is the surface pressure, $T_s$, $T_{0+}$, and $T_\infty$ are the surface temperature, the air temperature just above the surface, and the top temperature (temperature assigned to the pressure level $p=0$), respectively, $\varepsilon_{g\Delta\nu}$ is the surface emissivity, and $\tau^{f}_{\Delta\nu}(p, p')$ is the flux transmission function from a level $p'$ to the level $p$.

The integrals in eqs. (1) and (2) are approximated using the trapezoidal rule, apart from the contribution of the adjacent layers which is evaluated using a 2-point Gaussian quadrature. Thus, for example,

$$\begin{aligned}
&\int_{p_{i-1/2}}^{p_s} \tau^{f}_{\Delta\nu}(p_{i-1/2}, p') \frac{dB_{\Delta\nu}(T_{p'})}{dp'}\, dp' \\
&\simeq w_a \tau^{f}_{\Delta\nu}(p_{i-1/2}, p_a)[B_{\Delta\nu}(T_{p_i}) - B_{\Delta\nu}(T_{p_{i-1/2}})] \\
&+ w_b \tau^{f}_{\Delta\nu}(p_{i-1/2}, p_b)[B_{\Delta\nu}(T_{p_{i+1/2}}) - B_{\Delta\nu}(T_{p_i})] \\
&+ \tfrac{1}{2} \sum_{j=i+1}^{n} [\tau^{f}_{\Delta\nu}(p_{i-1/2}, p_{j-1/2}) + \tau^{f}_{\Delta\nu}(p_{i-1/2}, p_{j+1/2})] \\
&\times [B_{\Delta\nu}(T_{p_{j+1/2}}) - B_{\Delta\nu}(T_{p_{j-1/2}})]\,. \qquad (3)
\end{aligned}$$

Here, half-levels (layer boundaries) are marked with the sub-indices 1/2, 3/2,..., $n+1/2$, and full-levels (mid-layers) with the sub-indices 1, 2,..., $n$, starting from the top of the atmosphere. The two Gaussian sub-levels within the nearest layer are denoted as $p_a$ and $p_b$, and $w_a$ and $w_b$ are the corresponding weight factors. Both the half-level and full-level temperatures are utilized in the calculations, although the latter in evaluating the contribution of the adjacent layers only.

In preliminary tests with the ECMWF radiation code, a certain "convergence problem" was encountered. It turned out to be impossible to use such a dense resolution that using an even denser grid would have introduced only insignificant changes in longwave fluxes. This behaviour was related to the temperature corrections made to the effective amounts of absorbers entering the calculation of transmission functions. As the convergence problem was quite a vexing one for vertical resolution studies, it was desirable to remove it. This was achieved by introducing a simple modification in the calculation of the temperature correction factors, see Section 8 for details. All ECMWF results given in the following sections were calculated with this modified version of the code. It is emphasized that the reason for modifying the code was to remove the resolution dependence related to the temperature corrections, not to improve the temperature dependence of absorption as such. Furthermore, while the modification is important for this study, its impact at resolutions typical for atmospheric models (around 1 $Wm^{-2}$ or less in radiative fluxes) is quite small compared to the usual errors of wide-band radiation schemes.

In the DWD scheme, the delta-two-stream method is used also in the longwave calculations, which enables explicit treatment of absorption, emission and scattering. Here, it is worth noting that, while negligible in the clear-sky cases, longwave scattering can be significant in cloudy situations. Ritter and Geleyn (1992) give an example where scattering reduces the outgoing longwave radiation by as much as 16 $Wm^{-2}$. In emissivity-type schemes, the effect of scattering can be implicitly parameterized, but as Ritter and Geleyn argue, only with partial success.

In each spectral interval, the transmission functions are approximated with sums of exponentials. A special method, the so-called fast exponential sum fitting technique (FESFT; see Ritter and Geleyn, 1992), is used to handle overlapping gas absorption in a computationally efficient way. The radiative transfer equation is solved separately for each term in the sums. The longwave fluxes exiting each layer are expressed as a linear combination of the incoming fluxes plus the change in the Planck function across the layer. Only the half-level temperatures are used in the calculations; within each layer, the Planck function is assumed to vary linearly with optical depth. The equations for the individual layers combine into a matrix equation, from which the radiative fluxes are solved. A noteworthy feature of this approach is that the computer time needed is linearly dependent on the number of layers, whereas in the emissivity-type method, the dependence is quadratic. This is demonstrated in Table 1 for a Sun workstation (a scalar computer). The figures given include also solar calculations for half of the grid points, and indicate that the two schemes are equally fast for a resolution of about 40 layers.

Table 1. *CPU time requirement of the ECMWF and DWD schemes on a Sun workstation (a scalar computer) as a function of the number of layers (ms/grid point)*

| Layers | 10 | 20 | 30 | 50 | 70 | 100 |
|---|---|---|---|---|---|---|
| ECMWF | 18 | 52 | 105 | 267 | 500 | 1040 |
| DWD | 42 | 84 | 129 | 213 | 288 | 416 |

For longwave calculations only, the schemes were equally fast for about 27–28 layers.

## 3. Data and methods

### 3.1. Data

Two different sets of atmospheric profiles were utilized. First, calculations were made for the 5 McClatchey et al. (1971) atmospheres (tropical, mid-latitude summer, mid-latitude winter, sub-arctic summer and sub-arctic winter). These profiles of temperature, humidity and ozone have been used extensively in the ICRCCM comparison (Ellingson et al., 1991). However, as the profiles are quite smooth, tests made only for them might, at least in some respects, lead to too optimistic conclusions about the effects of vertical discretization. Therefore, calculations were also made for a set of very detailed sounding profiles.

The set of detailed soundings consists of 24 temperature and humidity profiles measured at the Jokioinen Observatory in southern Finland (23.5 °E, 60.8 °N) using fast-response Vaisala radiosondes. For each month of the year 1994, the local night-time (00 UTC) sounding on the 1st and day-time (12 UTC) sounding on the 15th day of the month were sampled. In these soundings, temperature and humidity are reported at intervals of 10 s in time (about 60 m in height). The profiles extend to about 25 mb, above which a gradual change to a subjectively chosen McClatchey et al. profile was made. The ozone profile was also taken from the selected McClatchey et al. atmosphere. In Fig. 1, the atmospheric profiles are characterized with surface temperature and total water vapour amount. The profiles measured at Jokioinen can be seen to cover quite a wide range of atmospheric conditions, although, due to the northern location, many of them are relatively cold and dry.

The discretization of the temperature, humidity and ozone profiles was made in two phases. First, these quantities were specified in an extremely dense grid with 1688 layers. Here, a detail worth mentioning is that the temperature and humidity profiles of the McClatchey et al. atmospheres were approximated analytically, using functions suggested in the ICRCCM instructions. Second, the values of these quantities in the grids actually used in the calculations were specified by mass-

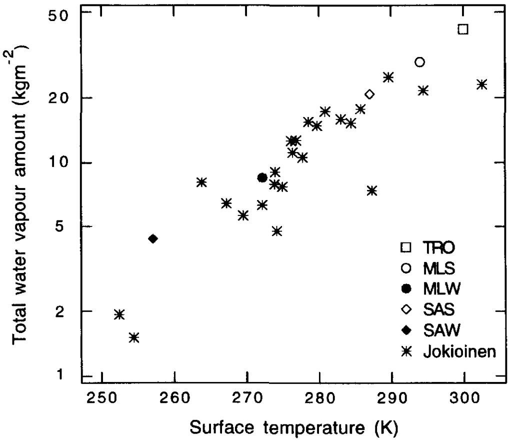


*Fig. 1.* Surface temperature and total water vapour amount for the 5 McClatchey et al. atmospheres (TRO: tropical; MLS: mid-latitude summer; MLW: mid-latitude winter; SAS: sub-arctic summer; SAW: sub-arctic winter) and for the 24 Jokioinen soundings.

conservative interpolation. That is, for each grid and each layer, the full-level (mid-layer) temperature, specific humidity and specific ozone content were defined as their average values within that layer, and were integrated numerically in the grid with 1688 layers. The half-level (layer boundary) temperatures are generally not predicted by atmospheric models, but have to be interpolated using the full-level temperatures. In this study, a linear change of temperature with the logarithm of pressure between the nearest full-levels was assumed. While we consider this method quite reasonable, the choice is admittedly somewhat arbitrary. Using a different interpolation method could slightly alter some of the results presented in Section 4.

The temperature assigned to the uppermost half-level (pressure level zero) was determined using the approach in the operational ECMWF model: within the highest layer, temperature was assumed to vary linearly with pressure. The air temperature just above the surface was assumed to be equal to the ground temperature, unless otherwise stated, and the surface emissivity was taken to be 1. In addition to $H_2O$ and $O_3$, $CO_2$ (300 ppmv for the McClatchey et al. profiles, 353 ppmv for the Jokioinen soundings), $CH_4$ (1.465/1.725 ppmv) and $N_2O$ (0.263/0.310 ppmv) were taken into account*. Finally, however humid the actual atmospheric profile, all cases were assumed to be cloud-free.

### 3.2. *Methods*

The basic approach is simple. For each situation considered, the calculations were first made in a very high resolution grid, a so-called reference grid. Then, the calculations were repeated in a set of coarser grids. The difference between the fluxes in the "coarse" grid and in the reference grid

$$\Delta F = F_{\text{coarse grid}} - F_{\text{reference grid}} \quad (4)$$

was then defined to be the error due to vertical discretization.

The discretization errors of radiative fluxes were determined at every half-level of the coarser grids. In cases where the half-level did not coincide with any of the half-levels in the reference grid, the reference grid fluxes were interpolated to that level, assuming that they change linearly with pressure. The errors in radiative heating or cooling rates in the coarser grids were calculated by evaluating the change of net flux discretization error within each layer.

After some experimentation, it was decided to use a grid with 366 layers as the reference grid. In this grid, the layer thickness was 2 mb from 1000 to 900 mb, 5 mb from 900 to 100 mb, and 0.005 mb above 0.1 mb**. Between 100 and 0.1 mb, the change of the logarithm of pressure across each layer was approximately constant (i.e., $\Delta \ln p \approx 0.05$). A few cases were also looked at with the extreme resolution of 1688 layers. The changes in radiative fluxes compared to the grid with 366 layers were generally well below 0.1 $Wm^{-2}$ even for the detailed sounding profiles.

In the following, results for 39 coarser grids are given. These grids are described in Table 2, which the reader is recommended to read carefully. The grids fall into two categories. The larger category, grids 1–33, was used to study systematically the effect of coarsening resolution in different parts of the atmosphere. These grids are identical to the reference grid elsewhere, but coarser in one particular slice of the vertical column. This slice is divided successively into 1, 2, 4, or more layers (below 200 mb, layers with equal $\Delta p$ were used, above that, layers with equal $\Delta \ln p$). Grids 1–6 address the significance of resolution in the lowest atmosphere (800–1000 mb), and grids 7–10, 11–14, 15–18, 19–22, 23–25 and 26–28 that in the slabs 600–800, 400–600, 200–400, 50–200, 10–50, and 1–10 mb, respectively. The effect of changing the thickness of the uppermost layer was investigated using grids 29–33.

The "systematic grids" 1–33 are, of course, not as such useful in atmospheric models. Therefore, calculations were also made in several grids with more typical numbers of layers; results for six of them are reported here. 5 of these "realistic grids" are grids actually used in weather prediction or climate models (35–39). The additional one (34) is a "basic grid", in which all the tropospheric layers have equal $\Delta p$ and all the stratospheric layers equal $\Delta \ln p$.

## 4. Results

### 4.1. *Long-wave fluxes*

The errors caused by vertical discretization in the downward longwave flux at the surface and the upward longwave flux at the top of the atmosphere (TOA) are displayed in Figs. 2 and 3, respectively. The results are shown for each grid and each atmospheric profile studied, and separately for the ECMWF and DWD radiation codes. To start with, the results in the systematic grids 1–33 are considered.

The downward flux at the surface is most sensitive to the resolution in the lowest atmosphere, that is, in the slab 800–1000 mb (grids 1–6). On the other hand, the resolution above the 600 mb level (grids 11–33) has a virtually negligible effect. These features are, of course, expected: the major part of the thermal radiation reaching the surface is known to originate from the humid layers close to the ground. In both the ECMWF and DWD schemes, the discretization causes, in most cases, the downward flux at the surface to decrease. A striking feature is that the spread of errors for the Jokioinen soundings is much larger

* The reason for using the mentioned $CH_4$ and $N_2O$ concentrations is that in the DWD scheme, these gases are not treated separately but as components of a "hybrid-$CO_2$", see Ritter and Geleyn (1992). Thus, their concentrations cannot be defined independently.

** The grids are given here for a surface pressure of 1000 mb. In order to adjust the grids to the actual surface pressure $p_s$ (which varied between 963 and 1022 mb), the layers were simply stretched by the factor $p_s/1000$.

Table 2. *The 39 coarser grids, given for a surface pressure of 1000 mb*

**Systematic grids**

| | | | |
|---|---|---|---|
| 1: | 1 layer between 800 and 1000 mb | 19: | 1 layer between 50 and 200 mb |
| 2: | 2 layers between 800 and 1000 mb | 20: | 2 layers between 50 and 200 mb |
| 3: | 4 layers between 800 and 1000 mb | 21: | 4 layers between 50 and 200 mb |
| 4: | 8 layers between 800 and 1000 mb | 22: | 8 layers between 50 and 200 mb |
| 5: | 16 layers between 800 and 1000 mb | 23: | 1 layer between 10 and 50 mb |
| 6: | 32 layers between 800 and 1000 mb | 24: | 2 layers between 10 and 50 mb |
| 7: | 1 layer between 600 and 800 mb | 25: | 4 layers between 10 and 50 mb |
| 8: | 2 layers between 600 and 800 mb | 26: | 1 layer between 1 and 10 mb |
| 9: | 4 layers between 600 and 800 mb | 27: | 2 layers between 1 and 10 mb |
| 10: | 8 layers between 600 and 800 mb | 28: | 4 layers between 1 and 10 mb |
| 11: | 1 layer between 400 and 600 mb | 29: | Thickness of the uppermost layer 100 mb |
| 12: | 2 layers between 400 and 600 mb | 30: | Thickness of the uppermost layer 30 mb |
| 13: | 4 layers between 400 and 600 mb | 31: | Thickness of the uppermost layer 10 mb |
| 14: | 8 layers between 400 and 600 mb | 32: | Thickness of the uppermost layer 3 mb |
| 15: | 1 layer between 200 and 400 mb | 33: | Thickness of the uppermost layer 1 mb |
| 16: | 2 layers between 200 and 400 mb | | |
| 17: | 4 layers between 200 and 400 mb | | |
| 18: | 8 layers between 200 and 400 mb | | |

**Realistic grids**

| | |
|---|---|
| 34: | Basic grid (21, 8, 13)<br>(0, 100, 156, 242, 376, 585, 909, 1414, 2199, 3420, 5318, 8270, 12861, 20000, 30000, 40000, 50000, 60000, 70000, 80000, 90000, 100000) |
| 35: | The LMD GCM (Laboratoire de Météorologie Dynamique) grid (11, 8, 3)<br>(0, 3800, 10600, 20800, 34000, 48900, 63800, 77000, 87300, 94100, 97900, 100000) |
| 36: | The DWD Global Model grid (19, 12, 7)<br>(0, 2000, 4000, 6080, 8604, 11917, 16259, 21764, 28453, 36236, 44909, 54162, 63595, 72738, 81095, 88194, 93658, 97299, 99228, 100000) |
| 37: | The DWD Europa-Model grid (20, 16, 4)<br>(0, 5000, 10000, 16000, 22000, 28000, 34000, 40000, 46500, 53500, 60000, 66000, 72000, 78000, 84000, 89000, 92500, 95000, 97500, 99200, 100000) |
| 38: | The ARPEGE GCM grid (30, 10, 20)<br>(0, 2, 11, 31, 76, 151, 267, 468, 688, 913, 1204, 1590, 2099, 2770, 3655, 4821, 6352, 8429, 11101, 14624, 18568, 26000, 39100, 52300, 62900, 73500, 83000, 91650, 96120, 98990, 100000) |
| 39: | The ECMWF grid (31, 24, 7)<br>(0, 2457, 4948, 7500, 10142, 12882, 15748, 18750, 21907, 25202, 28666, 32275, 36024, 39922, 43940, 48070, 52289, 56566, 60881, 65193, 69480, 73685, 77776, 81705, 85406, 88834, 91934, 94627, 96861, 98550, 99620, 100000) |

The "systematic grids" 1–33 are identical to the reference grid apart from the exception mentioned. The three figures given in parenthesis after the name of each of the "realistic grids" 34–39 are the total number of layers, the number of layers below the tropopause (taken to be at 200 mb), and the number of layers above the tropopause, respectively. After that, the location of the half-levels (in Pa) is listed.

than that for the McClatchey et al. profiles. The largest errors were found in cases with sharp surface inversions. A more thorough discussion of this feature follows in Section 5.

The largest errors of the upward flux at the TOA occur in grid 15, which has only one layer between 200 and 400 mb. The differences in the relative importance of resolution in different parts of the vertical column are, however, smaller than in case of the downward flux at the surface. This is consistent with the fact that in different spectral regions, the major contribution to the outgoing longwave radiation comes from different parts of the atmosphere, see Plate 4 in Clough et al. (1992) for water vapour.

In the DWD scheme, the effect of coarse tropo-

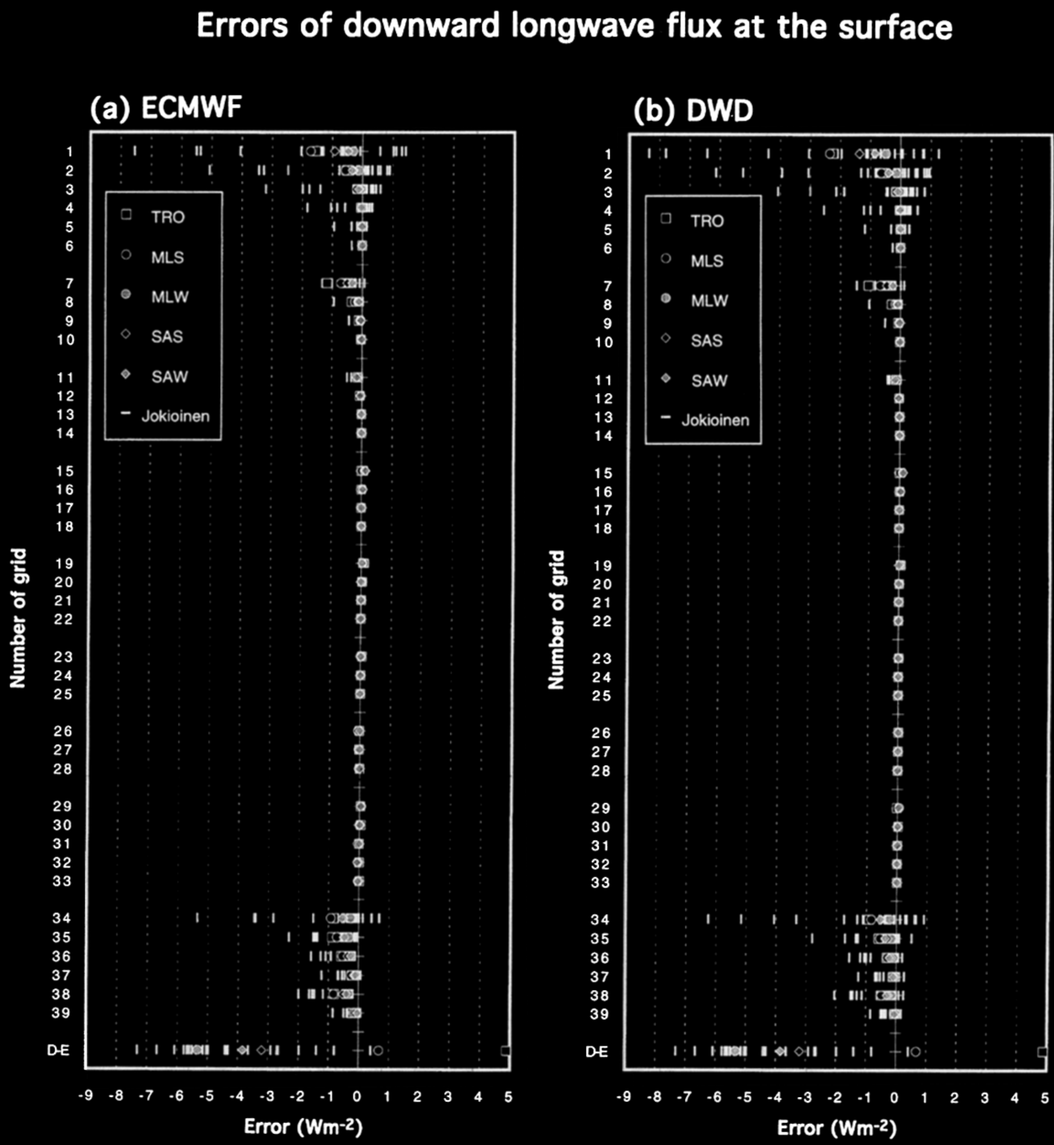


*Fig. 2.* Discretization errors of the downward longwave flux at the surface ($Wm^{-2}$) in the 39 coarser grids for the five McClatchey et al. atmospheres and the 24 Jokioinen soundings. Lowermost ("D-E") is shown the difference between the DWD and ECMWF results in the reference grid. (a) Results for the ECMWF scheme. (b) Results for the DWD scheme.

spheric resolution is to systematically decrease the upward flux at the TOA. This is probably due to the assumption that the Planck function varies linearly with optical depth, which corresponds roughly to the case where the amounts of absorbing gases are constant within each layer. However, in the troposphere both the temperature and $H_2O$ concentration generally decrease with height. Thus, in effect, vertical discretization acts here to "transfer" water vapour to the upper (colder) part of each layer, leading to slightly smaller upward flux.

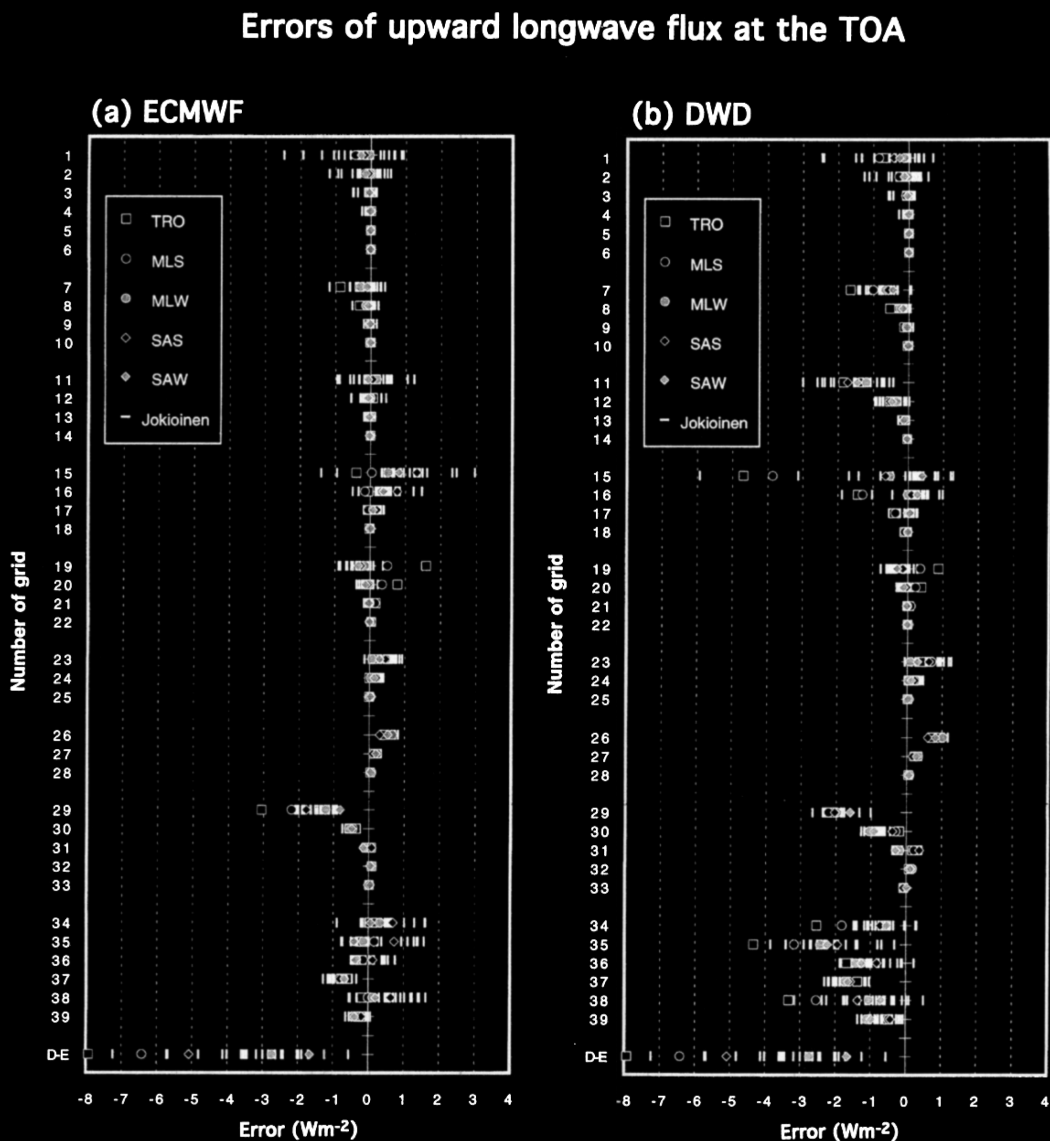


*Fig. 3.* As Fig. 2, but for the upward longwave flux at the top of the atmosphere.

In the ECMWF scheme, depending on the case, coarse tropospheric resolution leads either to decreased or increased upward flux at the TOA. The explanation for the lack of systematic behaviour is probably the following: When the upward flux is calculated (from eq. (1)), the contribution of all layers but the uppermost one is evaluated using the trapezoidal rule. This rule gives accurate results when the transmission functions depend linearly on the Planck function within each layer. However, the dependence of transmission functions on optical depth is non-linear. In fact, assuming the vertical temperature gradient to be approximately constant, linear dependence of $\tau^{f}_{\Delta\nu}(0, p')$ on the Planck function can only be achieved if the concentrations of absorbing gases increase with increasing pressure. Qualitatively, this corresponds to the typical water vapour distribution in the troposphere. A more detailed discussion of the numerical aspects of different formulations of the emissivity-type method can be found in Ridgway et al. (1991).

In grids with coarsened resolution in the stratosphere (23–28), the errors of the upward flux at the TOA are positive in both schemes. However, the opposite is true if the uppermost layer is very thick (grids 29, 30). This latter feature may be sensitive to the exact method of determining the temperature at the uppermost half-level. On the whole, the fact that coarse resolution in different parts of the atmosphere tends to have opposite effects on the upward flux at the TOA suggests that some compensation of errors is likely to happen when real grids with relatively coarse resolution throughout the vertical column are used.

The results for the net longwave flux at the tropopause level (not shown) were rather similar to those for the upward flux at the TOA. The clearest difference was that the effect of middle and upper stratospheric resolution was smaller.

The results obtained in the realistic grids (34–39) are, at least qualitatively, consistent with those obtained in the systematic grids. In both schemes, the discretization error of the downward flux at the surface is generally negative. The same is true also for the upward flux at the TOA in the results of the DWD scheme. The ECMWF scheme, however, shows such a systematic feature only for grid 37, in which the highest layer is as thick as 50 mb.

Quantitatively, the discretization error of the downward flux at the surface is, in most cases, within 1 $Wm^{-2}$ for each of the "real" grids (35–39), and both for the ECMWF and DWD schemes. (This is true also for the basic grid (34), even though the error is much larger in some cases.) With the ECMWF scheme, equally good results are obtained also for the upward flux at the TOA and the net flux at the tropopause. In fact, the discretization error of net flux remains generally below 2 $Wm^{-2}$ throughout the vertical column (Table 3). For the DWD scheme, the discretization errors of the upward flux at the TOA and the net flux at the tropopause, as well as the maximum errors of net flux are typically somewhat larger than those for the ECMWF scheme. However, for example in the DWD grids 36 and 37, even the maximum errors are in most cases less than 2 $Wm^{-2}$. This holds also for the total longwave divergence. Thus it seems that given these two radiation codes, it is possible to keep the discretization errors within about 2 $Wm^{-2}$, if the grid has about 20 judiciously selected levels, a conclusion, which is somewhat more optimistic than that reached by Morcrette and Fouquart (1985) cited in the introduction.

As for the "judicious" selection of levels, it appears that as long as interest is centred on calculating radiative fluxes (and not on resolving the fine details of the middle atmospheric cooling rate profile), it is preferable to have the majority of the layers in the troposphere. Some confidence in this conclusion can be obtained, for example, by comparing the errors in the ARPEGE grid (38) to those in grids 36, 37, and 39. Further tests (not shown) also supported this notion. The relatively small effect of stratospheric resolution on radiative fluxes is probably a direct consequence of the vertical distribution of mass in the atmosphere.

As a rough yardstick of the magnitude of errors

Table 3. *The maximum (positive or negative) net longwave flux discretization error in the real grids (35–39): (a) the average value ($Wm^{-2}$), calculated separately for the 5 McClatchey et al. (1971) profiles and the 24 Jokioinen soundings; (b) the absolute maximum value ($Wm^{-2}$); (c) the number of cases (out of 29) where the error exceeded 2 $Wm^{-2}$*

| | 35: LMD | | 36: DWD GM | | 37: DWD EM | | 38: ARPEGE | | 39: ECMWF | |
|---|---|---|---|---|---|---|---|---|---|---|
| | EC | DWD | EC | DWD | EC | DWD | EC | DWD | EC | DWD |
| (a) Average | | | | | | | | | | |
| McClatchey | 1.5 | 3.5 | 0.6 | 1.7 | 0.7 | 1.7 | 0.9 | 2.2 | 0.3 | 1.0 |
| Jokioinen | 1.7 | 2.9 | 1.1 | 1.7 | 0.9 | 1.8 | 1.5 | 2.3 | 0.6 | 0.9 |
| (b) Maximum | 2.8 | 5.6 | 2.5 | 2.4 | 1.9 | 2.3 | 2.7 | 4.3 | 1.4 | 1.6 |
| (c) Error >2 $Wm^{-2}$ | 7 | 24 | 1 | 7 | 0 | 8 | 3 | 15 | 0 | 0 |

that arise from factors other than vertical discretization, the difference between the DWD and ECMWF results in the reference grid is displayed at the lowermost row in Figs. 2, 3. Without going into any fine details, it is seen that for typical grids of 20 layers or so, the discretization errors are generally smaller, often much smaller, than the difference between the two schemes. This suggests that, at least for these two radiation schemes, vertical discretization is a relatively small source of error, unless very coarse grids are used.

It was noted earlier that some of the Jokioinen soundings showed substantially larger errors of downward flux at the surface than the McClatchey et al. profiles when there was poor resolution in the boundary layer. Even for the real grids (35–39), the range of errors of this quantity is significantly larger for the Jokioinen soundings than for the McClatchey et al. (1971) profiles. The mean errors, however, were found to be only marginally different for these two data sets. Concerning the upward flux at the TOA, the DWD scheme was found to give on the average slightly more negative (larger) errors for the McClatchey et al. (1971) profiles than for the Jokioinen soundings. Noting that the errors obtained for the McClatchey et al. (1971) profiles tend to increase with increasing temperature and humidity, this feature is most probably a consequence of the relative coldness of the Jokioinen data set rather than any profound difference between detailed and smooth atmospheric profiles.

For the ECMWF scheme, the average value of maximum net flux error is larger for the Jokioinen soundings than for the McClatchey et al. (1971) profiles, by at most a factor of two (Table 3). For the DWD scheme, however, the difference between the two data sets is very small. In part, this suggests that the dominant contribution to the total error comes from the systematic tendency of the upward flux to decrease when tropospheric resolution is made coarser, rather than from random errors related to subgrid-scale details. Partially, however, the results may be biased by the coldness of the Jokioinen data set. If very warm and humid profiles were added to the set of detailed soundings, the average maximum errors would probably increase somewhat. Even so, the difference between detailed and smooth sounding profiles would hardly be drastic.

### *4.2. Longwave cooling rates*

Qualitatively, the most prominent systematic features of longwave cooling rate discretization errors were that (1) around the tropopause, coarse resolution led to increased cooling, and (2) specially for the DWD scheme, cooling rates in the upper troposphere were decreased. The former feature is obviously related to the fact that discretization tends to smooth the tropopause (i.e., make it too warm). The latter is probably mainly associated with the "transfer" of water vapour to upper (colder) parts of the layers, which was discussed in subsection 4.1.

In order to get a more quantitative view, the root-mean-square discretization errors of longwave cooling rate were computed for each layer in grids 34–39, separately for the five McClatchey et al. (1971) atmospheres and the 24 Jokioinen soundings. In Fig. 4, the results for pressures larger than 10 mb are shown for 5 grids, together with the rms-difference between the DWD and ECMWF results in the reference grid (panel (f)). In agreement with the systematic features discussed above, the rms error profiles for the McClatchey et al. (1971) atmospheres show a maximum around, or somewhat below, the tropopause region. In grids with coarse resolution in the upper troposphere (the basic grid 34, the LMD grid 35 and the ARPEGE grid 38), the errors approach 0.1 K/d for the ECMWF scheme and slightly exceed that for the DWD scheme. In the middle and lower troposphere, the typical magnitude of errors ranges from about 0.01 K/d in the ECMWF grid (39) to about 0.05 K/d in the LMD grid. In most of the grids present in Fig. 4, stratospheric resolution is relatively coarse. This is reflected in cooling rate errors that are typically slightly larger than those in most of the troposphere, though generally below 0.1 K/d. Based on these tests only, it is hard to give any general advice on how fine the stratospheric resolution used in atmospheric models should be. A fact that should be borne in mind in climate modelling, though, is that the lower stratosphere is close to radiative equilibrium, especially in the tropics; therefore, high accuracy in radiation calculations is required (Olaguer et al., 1992).

The cooling rate discretization errors for the McClatchey et al. profiles can be attributed to deficiencies in describing the effects of the system-

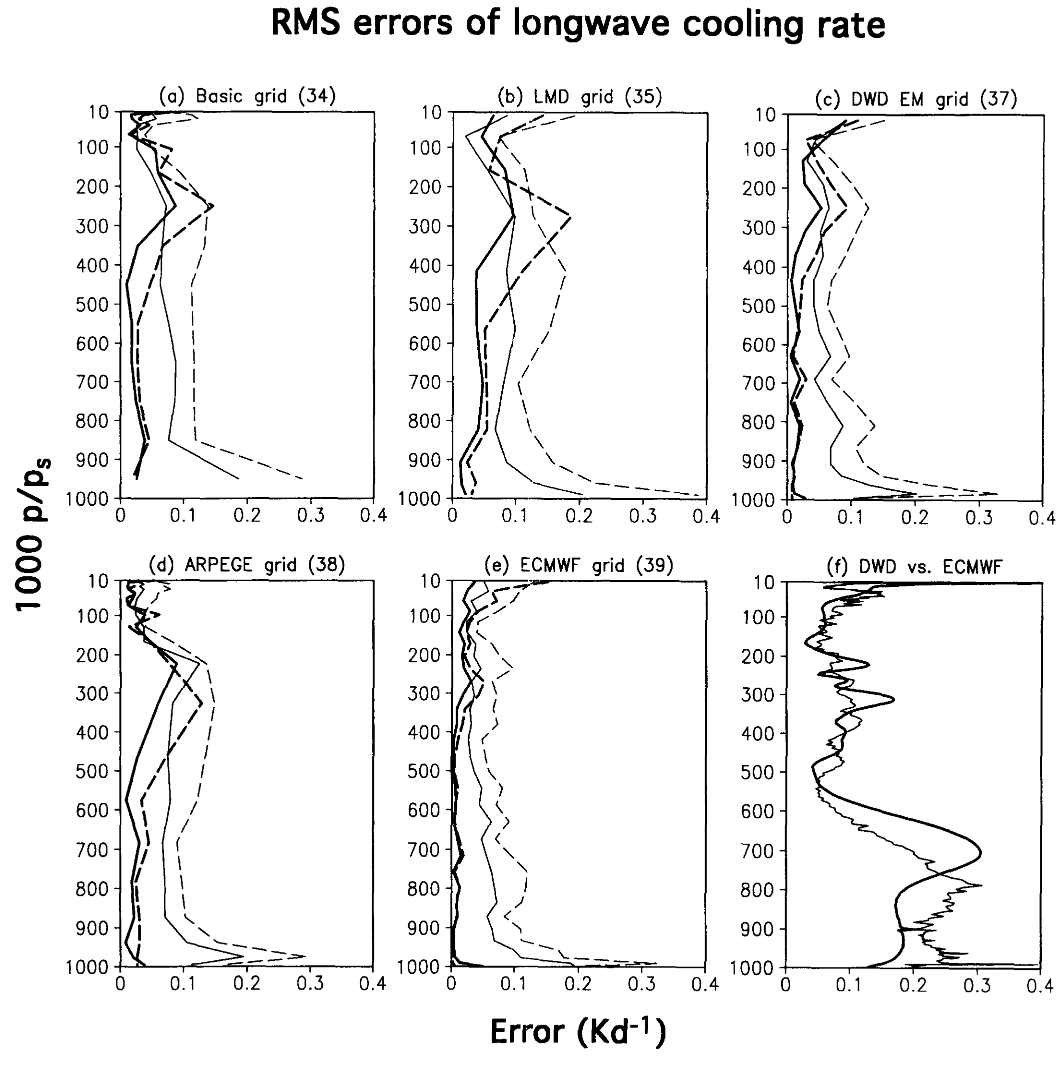


*Fig. 4.* (a)–(e). Root-mean-square discretization errors of longwave cooling rate (K/d) in five grids. Results shown separately for the five McClatchey et al. atmospheres (thick lines) and the 24 Jokioinen soundings (thin lines), and for the ECMWF (solid lines) and DWD (dashed lines) radiation codes. (f) The rms-difference between the ECMWF and DWD reference grid results, separately for the McClatchey et al. atmospheres (thick line) and Jokioinen soundings (thin line).

atic changes of temperature and gas concentrations with height. The errors for the Jokioinen soundings, however, also include the contribution of the random effects related to small-scale details of the profiles, and are therefore larger, particularly in the middle and lower troposphere. Apart from the boundary layer where there is a pronounced maximum, the rms errors for the Jokioinen soundings are typically around or slightly below 0.1 K/d. The errors decrease with increasing resolution, but more slowly than those for the McClatchey et al. profiles.

The cooling rate discretization errors are generally somewhat larger for the DWD than for the ECMWF scheme. To some extent, this may be explained by the systematic errors related to the "transfer" of water vapour to the upper (colder) parts of the layers in the DWD scheme. Another factor, which seems more important at least for the results obtained for the Jokioinen soundings, is that the full-level temperatures are utilized in the ECMWF scheme only.

The typical discretization errors are of roughly the same magnitude as the rms difference between the cooling rates calculated with the ECMWF and DWD schemes (Fig. 4f) between about 50 and 500 mb only. Elsewhere, the difference between the two codes dominates by a substantial marginal. (An exception are the results for the Jokioinen soundings in the boundary layer.) The lower mid-tropospheric maxima in the rms difference of about 0.3 K/d result from systematically larger cooling rates in the ECMWF than in the DWD scheme in that part of the vertical column.

While both schemes have been originally designed to be used at pressures larger than about 10 mb, the ECMWF scheme presently includes a simplified Voigt line shape (Giorgetta and Morcrette, 1995), which significantly extends its domain of applicability in the vertical. For this scheme, therefore, we also briefly looked at the cooling rate discretization errors in the upper stratosphere. Both in the basic grid (34) and in the ARPEGE grid (38), the errors showed a substantial increase near the stratopause (1 mb), reaching a magnitude of about 0.5 K/d. Here, it is worth noting that longwave cooling rates near the stratopause are very large (about 10 K/d) compared to those lower in the atmosphere.

We conclude this section by schematically demonstrating a problem that may arise in radiation schemes where the full-level temperatures are not used in evaluating the Planck function. In Fig. 5 are shown longwave cooling rates in the basic grid (34) for (1) the (unperturbed) Mid-latitude summer atmosphere and (2) a perturbed profile, where the temperature is 2 K higher (lower) at even (odd) full-levels. In the ECMWF scheme, the perturbation leads, as it should, to increased (decreased) cooling in layers with increased (decreased) temperature. The results of the DWD scheme are, however, virtually identical for the two profiles, as the perturbation does not appreciably affect the (interpolated) half-level temperatures. The potential implication is that if there is, for some reason, unnatural small-scale noise in the vertical temperature profile in an atmospheric model, a radiation code that uses the half-level temperatures only is not able to damp it adequately. This kind of "two-grid-wave oscillation" problem was actually encountered at the ECMWF some years ago, and was, in fact, the main reason for incorporating the full-level temperatures into the present version of the ECMWF radiation code (Jean-Jacques Morcrette, personal communication). Lastly, it should be stressed that two-stream methods are not inherently inferior to emissivity-type methods in this aspect of radiative transfer modelling. Shibata and Uchiyama (1994) have recently described how to incorporate both the full- and half-level temperatures not only into two-stream approximations, but also into $N$-stream methods in general.

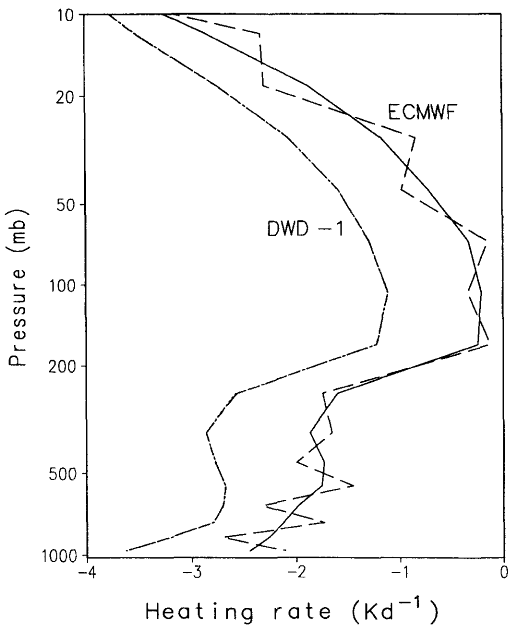


*Fig. 5.* Longwave heating rates (K/d) for unperturbed and perturbed (see text) Mid-latitude summer atmospheres. Solid line: ECMWF/unperturbed; dashed line: ECMWF/perturbed; dotted line: DWD/unperturbed; dash-dotted line: DWD/perturbed. For clarity, the DWD results are shifted by −1 K/d.

### *4.3. Shortwave results*

As far as the author is aware, no remarks concerning the resolution dependence of clear-sky shortwave calculations have been published in the meteorological literature. The results obtained in this study do not support the notion that this topic should be one of utmost importance, either. In particular, the discretization errors of shortwave fluxes produced by the DWD scheme were typically of the order of 0.1 $Wm^{-2}$ only, given that the amounts of the absorbing gases in each layer were forced to be correct (i.e, interpolated in a mass-conserving fashion).

The errors were, however, somewhat larger for the ECMWF scheme. For example, the maximum error of the downward shortwave flux at the surface was over 2 $Wm^{-2}$ in the relatively coarse LMD grid (11 layers), and about 0.7 $Wm^{-2}$ in the operational ECMWF grid (31 layers). These errors depended considerably on the solar zenith angle, but only weakly on the atmospheric profile, and they were found to be related to the parameterization of Rayleigh scattering (see Fig. 6). The parameterization method of Rayleigh scattering used in the ECMWF scheme is that described in Fouquart (1988, pp. 267–270).

That vertical resolution has a smaller impact on clear-sky shortwave than longwave calculations is actually not surprising: the difficult problem of calculating the contribution of adjacent layers as sources of radiation is unimportant in the solar region, since the source indeed is the sun, scattering playing a relatively minor role in clear-sky conditions. Nonetheless, the treatment of molecular scattering causes some differences in the behaviour of different schemes, as seen in Fig. 6.

In order to put the discretization errors of shortwave fluxes into the correct perspective, a comparison of the ECMWF and DWD results is again worth considering. As shown in Fig. 6, the difference between the two codes in the downward shortwave flux at the surface amounts to about 20 $Wm^{-2}$ for the Mid-latitude summer atmosphere, when the sun is overhead. For a large part, this rather substantial difference is related to water vapour absorption (cf. Fig. 9 in Ritter and Geleyn, 1992); also, the effect of the minor absorbing gases $CO_2$, $O_2$, CO, $CH_4$ and $N_2O$ is larger in the DWD than in the ECMWF scheme. In this context, a relevant note is that the ECMWF scheme has been observed to overestimate the clear-sky solar flux at the surface by 5–10% (Betts et al., 1993).

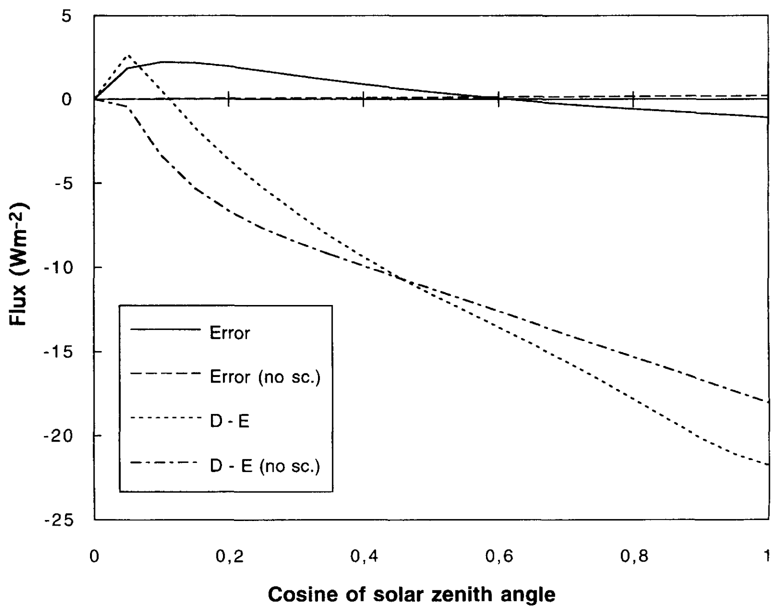


*Fig. 6.* Discretization error of the downward shortwave flux at the surface ($Wm^{-2}$) for the ECMWF scheme in the LMD grid (35) with (solid line) and without (dashed line) Rayleigh scattering. Also shown is the difference between the DWD and ECMWF results in the reference grid with (dotted line) and without (dash-dotted line) Rayleigh scattering. Mid-latitude summer atmosphere, surface albedo = 0.2.

However, it is unclear to what extent this can be explained by low gas absorption and to what extent by the fact that aerosols were neglected in the ECMWF model at that time. Overestimation of incoming solar flux at the surface seems, in fact, to be a fairly common problem (Garratt, 1994).

## 5. Inversion situations

It was noted in subsection 4.1 that rather large discretization errors of downward longwave flux at the surface occurred in inversion situations, if there was poor resolution in the boundary layer. The errors were negative, which can be best understood by considering a specific example. The sharpest surface inversion included in the random sample of 24 Jokioinen soundings was that in the 00 UTC 1 September profile, with a temperature change of 7.5 K in the lowest 100 m. This case also produced the largest discretization errors. The temperature and humidity profiles are shown in Figs. 7a and 7b, respectively; also given are the discretized profiles in the basic grid (34). In Fig. 7c, the discretization errors of longwave fluxes in this grid are displayed for the ECMWF scheme.

The reason for the negative error in the downward flux at the surface is evident from Fig. 7a: coarse discretization makes the inversion too thick. This also contributes to the fact that the discretization error of upward flux remains negative throughout the troposphere. Around the tropopause, however, the error changes sign, obviously due to the smoothing of the temperature profile. The humidity profile is likewise largely smoothed by discretization, but the detailed effects of this are not so easy to separate.

Apart from the aspects related to vertical discretization, the profiles of longwave fluxes and cooling rates in surface inversion situations are, as such, rather interesting. While longwave cooling in nocturnal inversions has been discussed by several authors (Fleagle and Businger, 1963; Kondo, 1971; André and Mahrt, 1982; Stull, 1988), a further example, summarizing the typical features, is worthwhile. Thus, consider the results of the ECMWF scheme for the same 00 UTC 1 September situation (Fig. 8). The results were

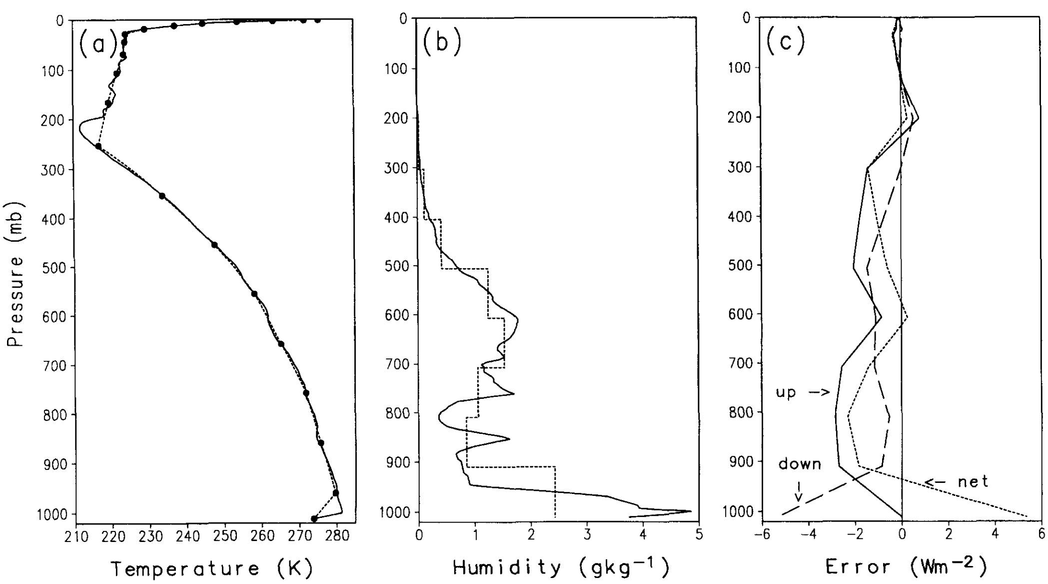


*Fig. 7.* (a) Temperature profile (K) for the Jokioinen 00 UTC 1 September 1994 sounding. Solid line: accurate profile; dotted line: discretized profile in the basic grid (34). The surface and full-level temperatures are marked with full circles. (b) Accurate (solid line) and discretized (dotted line) profiles of specific humidity (gkg$^{-1}$). (c) Profiles of longwave flux discretization errors (Wm$^{-2}$) for the ECMWF scheme.

now calculated in a grid with an extremely dense resolution near the surface: within the lowest 100 mb, there were 270 layers whose thickness decreased gradually from 2 mb to only $10^{-4}$ mb (0.8 mm!) in the lowermost layer.

In an overall picture of the radiative fluxes (Fig. 8a), the inversion manifests itself in maxima of upward and downward flux that are not located at the surface as usual, but in the vicinity of the top of the inversion. The results shown with solid lines are those for the case with no temperature discontinuity at the surface, whereas the dashed lines refer to a case where a discontinuity of 3 K (i.e., $T_s - T_{0^+} = -3$ K in eq. (1)) was assumed. (At least at Jokioinen, this is a typical value of the difference between the two meter and ground level minimum temperatures during clear nights.) The colder surface temperature in the latter case leads, naturally, to smaller upward and net flux. The difference compared to the case with no discontinuity (dotted line, magnified scale) decreases with height from nearly 14 $\mathrm{Wm^{-2}}$ at the surface to about 4 $\mathrm{Wm^{-2}}$ at the TOA. Remarkably, though not so surprisingly, considering that large parts of the longwave region are quite opaque, half of this change occurs within the lowest 4 mb. This implies that the temperature discontinuity induces strong radiative cooling near the surface, but has much less effect on air layers located higher up. Indeed, as shown in Fig. 8b, the strongest cooling is confined to the lowest millibar.

The average cooling rate of the lowest millibar was, however, found to be somewhat sensitive to the exact definition of the temperature profile just above the ground. In the (improbable) case of a step discontinuity of 3 K, a value of 24.2 K/d was obtained (dashed line). When, instead, the change was assumed to occur within the lowest two metres (the temperature obeying a logarithmic profile with a roughness length $z_0 = 1$ cm), the cooling rate dropped to 12.7 K/d (dotted line). Further tests (not reported) indicated, however, that about one half of this difference may be computational rather than physical.

Two further features in Fig. 8b are worth noting. First, in the case where there is no difference between the surface and 2-m temperatures (full line), the energy exchange with the warmer air layers above makes the lowest millibars experience radiative heating. Second, the top of the inversion (1000 mb) experiences a peak value of cooling rate of about 10 K/d. The sharpness of this feature may be, though, somewhat artificial. The fact that the sounding data were sampled at a resolution of about 6 mb only acts probably to exaggerate the abruptness of the change of the temperature gradient. The large cooling near the top of the inversion was noted also by André and Mahrt (1982). These authors suggest it to be the main reason for the tendency of inversion layers to thicken during nights.

Finally, Fig. 8c shows a close-up of the cooling rate profile in the lowest millibar ($\approx 8$ m). The results are those for the case with a logarithmic temperature profile in the lowest two metres, and are shown, for comparison, for both the ECMWF (solid line) and DWD (dashed line) radiation codes. In the ECMWF scheme, the cooling rate exceeds 10 K/d in the lowest 0.5 mb, and reaches a maximum of 31 K/d at about 0.03–0.04 mb ($\approx 30$ cm) above the ground. The apparent secondary maximum at 0.25 mb above the ground is an artifact resulting from a change of gradient in the assumed temperature profile at the two meter level. In the immediate vicinity of the surface, the warming effect due to energy exchange with air layers above starts to dominate, so that radiative heating takes place, analogously to the case with no difference between the surface and two meter temperatures. The DWD scheme gives slightly smaller cooling rates than the ECMWF scheme and also locates the maximum cooling slightly higher. Generally speaking, though, the two quite different schemes are in fairly good agreement. (This is, of course, not an absolute guarantee of their accuracy.)

The details of the surface layer radiative cooling profile were investigated also in a few other inversion cases. While the results were qualitatively similar from case to case, the maximum cooling rate was noted to increase with increasing humidity. For example, in a winter case with a surface specific humidity $q_s = 0.56$ g/kg, the maximum cooling rate given by the ECMWF scheme was only about 11 K/d, when a logarithmic temperature profile similar to that discussed above was assumed. On the other hand, in a summer case with $q_s = 9.2$ g/kg, a maximum value of 53 K/d was obtained. In an earlier study, Fleagle and Businger (1963, p. 200) calculated a maximum cooling rate of over 100 K/d for a case with $q_s \approx 8$ g/kg but a temperature profile steeper than

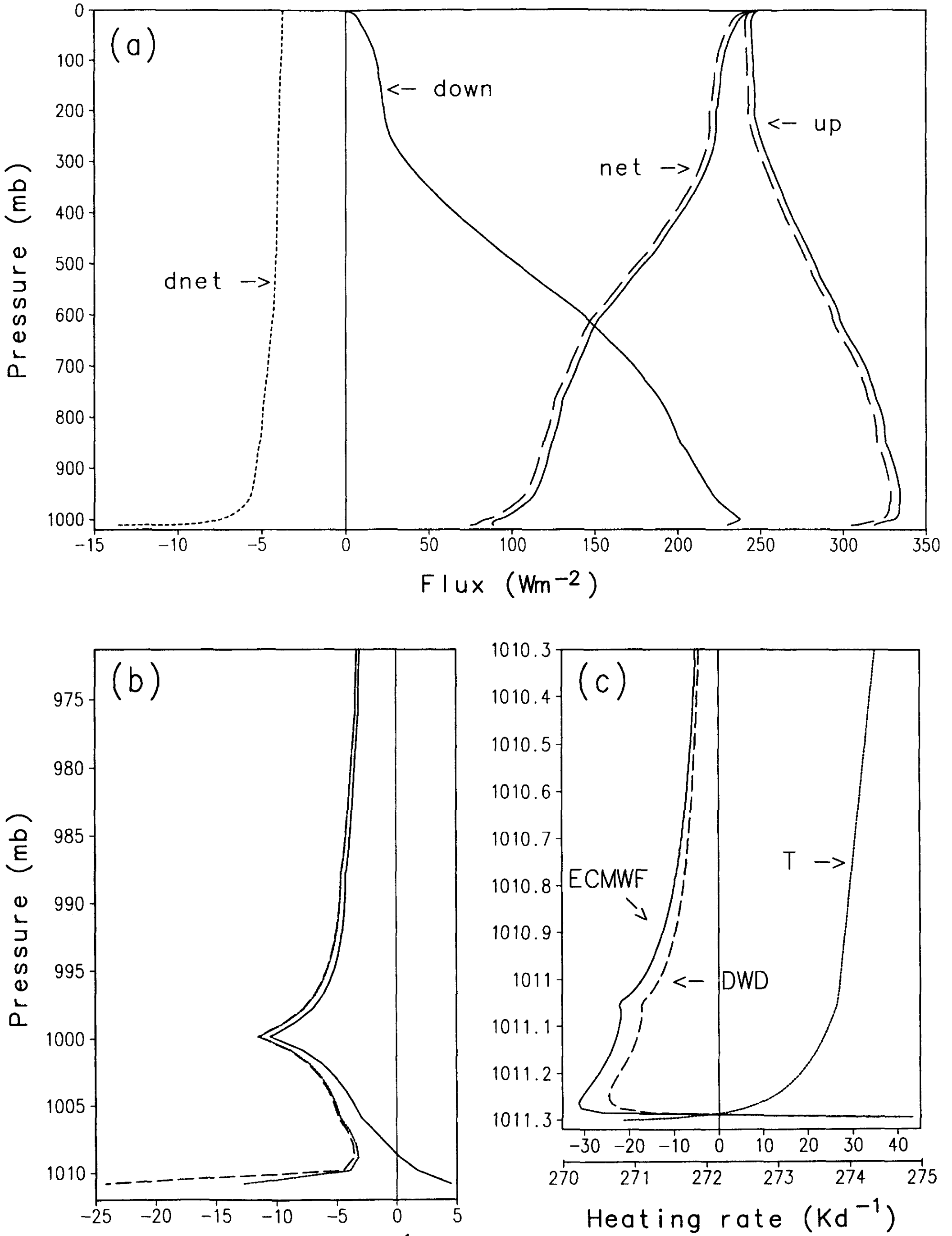
(a)
<– down
<– up
net –>
dnet –>
Pressure (mb)
Flux (Wm$^{-2}$)
(b)
Pressure (mb)
Heating rate (Kd$^{-1}$)
(c)
ECMWF
<– DWD
T –>
Heating rate (Kd$^{-1}$)
Temperature (K)

that discussed here. Radiative cooling rates of several degrees K/h have also been directly measured (Funk, 1960, 1962).

Of course, radiative cooling is not the only factor affecting the air temperature in inversions. In reality, there is always some turbulent mixing, the strength of which depends on stability and wind speed. This mixing works to smooth out the effect of radiative cooling, so that the actual cooling rate of surface air in inversion situations is often smaller than that due to radiation (Funk, 1960). The overall effect of turbulence on the boundary layer temperatures is, however, generally one of cooling. André and Mahrt (1982) conclude that for the inversion layer as a whole, clear-air radiative cooling and turbulent heat flux divergence are about equally important, although their vertical distribution is different. On the other hand, in the cases discussed by Carlson and Stull (1986) and Savijärvi (1991), turbulence made the larger contribution to the overall cooling. In addition to radiation and turbulence, subsidence and advection are forcing mechanisms that should be accounted for when studying inversions (Carlson and Stull, 1986).

Nevertheless, the above considerations highlight the potential importance of the radiative cooling induced by the colder ground in inversion situations. Another case, where the temperature difference between the surface and the air just aloft may have significant radiative effects, is the opposite one: sunny days with the ground warmer than air. As the temperature difference is often larger than that at night-time, the effect on radiative fluxes and heating rates can also be larger (cf. Kondo, 1971). While the boundary layer temperature profile is, in such situations, mainly determined by strong convective turbulent mixing, the temperature difference at the surface can have a considerable radiative impact on the overall energy balance, at least at extreme locations such as the Tibetan Plateau (Smith and Shi, 1992), or Mars (Savijärvi, 1991).

## 6. Summary and discussion

The sensitivity to vertical resolution of the clear-sky results produced by two radiation codes (a slightly modified version of the ECMWF scheme and the DWD scheme) was addressed. Results were calculated both for the five McClatchey et al. atmospheres and for a set of 24 fully detailed sounding profiles observed at Jokioinen, Finland.

As expected, the downward longwave flux at the surface was found to be most sensitive to resolution in the lower troposphere. For the upward flux at the TOA and net flux at the tropopause, the differences in the relative importance of resolution in different parts of the atmosphere were smaller. The rôle of upper tropospheric resolution was found to be rather pronounced, though. In both the ECMWF and DWD schemes, coarse vertical resolution led usually to decreased downward flux at the surface. In the DWD scheme, the discretization errors of the upward flux at the TOA were generally also negative, especially if there was coarse resolution in the upper troposphere. Such systematic features were, however, not present in the ECMWF results, probably due to compensation of errors.

For some of the Jokioinen soundings, the discretization errors of the downward flux at the surface were much larger than those for the McClatchey et al. (1971) atmospheres, if there was poor resolution in the boundary layer. The largest errors were associated with sharp surface inversions. Also in grids actually used in atmospheric models, the range of errors was somewhat larger for the Jokioinen soundings than for the McClatchey et al. (1971) profiles. However, the average errors of the longwave fluxes at the boundaries of the atmosphere were fairly similar for the two data sets. For the ECMWF scheme, the maximum errors of net longwave flux (i.e., largest positive or negative error within the vertical column) were on the average larger for the Jokioinen soundings than for the McClatchey et al. profiles, by at

*Fig. 8.* Results for the Jokioinen 00 UTC 1 September 1994 sounding. (a) Longwave fluxes for the ECMWF scheme ($Wm^{-2}$). Solid lines: no temperature discontinuity at the surface, dashed lines: a step discontinuity of 3 K. Dotted line: the effect of the discontinuity on the net flux (magnified scale). (b) Longwave heating (K/d) in the lowest 40 mb for the ECMWF scheme (plotting resolution 1 mb). Solid line: no temperature discontinuity at the surface, dashed line: a step discontinuity of 3 K; dotted line: logarithmic profile in the lowest two metres ($T_s - T_{2m} = -3$ K, $z_0 = 1$ cm). (c) Longwave heating in the lowest 1 mb for the case with logarithmic temperature profile (plotting resolution 0.01 mb). Solid line: ECMWF results; dashed line: DWD results, dotted line: temperature (K).

most a factor of two. For the DWD scheme, this difference was smaller.

Quantitatively, in grids with resolution typical to present-day atmospheric models, the discretization errors of longwave fluxes at the boundaries of the atmosphere and at the tropopause level were typically of the order of 1 $Wm^{-2}$ only. Moreover, it was found that about 20 layers were enough to keep even the maximum error of net longwave flux within 2 $Wm^{-2}$ in most cases. As long as interest is centred on calculating radiative fluxes (and not on resolving the fine details of the middle atmospheric cooling rate profile), it seems preferable to have the majority of the layers in the troposphere.

For the McClatchey et al. atmospheres, the longwave cooling rate discretization errors usually showed a maximum around or slightly below the tropopause, and reached a magnitude of 0.1 K/d in some of the real grids. In the middle and lower troposphere, and in most of the stratosphere, the errors were smaller. However, considerably larger errors occurred near the stratopause in those grids that extend to such low pressures. The errors obtained for the Jokioinen soundings generally exceeded those for the McClatchey et al. atmospheres, especially in the lower troposphere. In general, the cooling rate discretization errors were slightly larger for the DWD than for the ECMWF scheme.

The effect of vertical discretization on shortwave results was also investigated. Given the mass-conservative interpolation method, the errors were negligible (around 0.1 $Wm^{-2}$) for the DWD scheme, and small (usually below 1 $Wm^{-2}$) also for the ECMWF scheme.

Finally, the profiles of longwave fluxes and the respective cooling rates in surface inversion situations were discussed. The large magnitude, and the vertically confined nature, of the radiative cooling induced by a difference between the ground and surface air (two meter) temperatures was also demonstrated.

On the whole, the results are rather encouraging: with the typical resolution of present atmospheric models (20 layers or so), discretization errors can be kept at a moderately low level. The dominant contribution to the errors in clear-sky calculations comes generally from other factors, as was demonstrated by contrasting the differences between the ECMWF and DWD results with the errors caused by vertical discretization. Yet, only the direct radiative effects of discretization have been addressed in this study. In effect, it has been assumed that the model "knows" the state of the atmosphere exactly, and just presents it at a coarser resolution. In reality, changing the vertical resolution in an atmospheric model would affect the description of not only the radiative processes but also the hydrological cycle and atmospheric dynamics. These feedback effects of vertical discretization may act to distort the profiles of temperature and absorbing gases in a fashion that is not easy to determine.

Moreover, only clear-sky situations were considered, because it would be hard to conduct a study like this for cloudy-sky situations in a meaningful way. However, it seems plausible that the effects of vertical discretization might be larger in cloudy-sky than in clear-sky cases. In particular, clouds are often subgrid-scale (also) in the vertical, which certainly does not make it any easier to determine the location of clouds and other cloud parameters needed in radiation calculations. As stated by Geleyn (1981), this is one (though definitely not the only one) reason for the need to tune the cloud liquid water content in the often-used diagnostic (mainly relative humidity-based) cloud schemes. Furthermore, the distribution of radiative heating or cooling within clouds is known to be an important factor for the development of clouds in many cases (for references, see Hanson and Derr, 1987), but the resolution of the present atmospheric models is generally far too coarse to resolve it properly. It should be noted, though, that errors arising from factors other than vertical discretization are also likely to be larger in cloudy-sky than in clear-sky situations.

Lastly, there is the trivial fact that the effects of vertical discretization are model-dependent. This study should not be used as an excuse for totally neglecting to test the resolution sensitivity of other radiation schemes.

## 7. Acknowledgements

Jean-Jacques Morcrette and Bodo Ritter are thanked for providing the single column versions of the ECMWF and DWD radiation schemes, respectively, as well as for their useful comments. The comments and guidance obtained from

Hannu Savijärvi were also invaluable. The suggestions provided by the two anonymous reviewers are likewise acknowledged. Thanks are also due to Asko Tuominen from the Jokioinen Observatory for providing the sounding data.

## 8. Appendix

*The convergence problem*

Preliminary tests with the ECMWF radiation code showed that it was not possible to find out the values to which the longwave results are (possibly) converging when resolution is increased. In order to understand the nature of this problem, it is necessary to look at the parameterization of $H_2O$ and $CO_2$ transmission functions.

The transmission functions are parameterized using methods discussed in Morcrette et al. (1986). They depend on the linearly pressure-scaled, temperature-corrected effective absorber amount and have been developed into Padé approximants:

$$\tau^{f}_{\Delta\nu}(p, p') = \frac{c_0 + c_1\,(\beta u_e)^{1/2}}{d_0 + d_1(\beta u_e)^{1/2} + \beta u_e}. \tag{A.1}$$

Here, $\beta = 1.66$ is the diffusivity factor. The effective absorber amount $u_e$, for example for a slab extending from the top of the layer $i$ to the bottom of the layer $j$, is

$$u_e(p_{i-1/2}, p_{j+1/2}) = \frac{1}{g}\sum_{k=i}^{j} q_k \frac{p_k}{p_0} f_k \Delta p_k, \tag{A.2}$$

where $g$ is the acceleration of gravity, $q_k$ is the concentration of either $H_2O$ or $CO_2$ in the layer $k$ (kg/kg), $p_0$ is a reference pressure, $p_k$ is the pressure at the $k$th full-level, $\Delta p_k$ is the pressure thickness of the layer, and $f_k$ is a factor that accounts for the change of absorption coefficients with temperature. The functional form of these temperature correction factors is a generalization of that proposed by Rodgers and Walshaw (1966):

$$f_k = \exp[a(\overline{up})(T_k - 250) + b(\overline{up})(T_k - 250)^2]. \tag{A.3}$$

The regression coefficients $a$ and $b$ are parameterized as a function of the pressure-scaled absorber amount $\overline{up}$ in order to account for the fact that the temperature dependence of the transmission functions is considerably different for small and large absorber amounts (see Fig. 3 in Morcrette et al., 1986).

Ideally, the quantity $\overline{up}$ (and thus also the effective absorber amount $u_e$) should be evaluated separately for each level pair $(p, p')$ for which the transmission functions are to be calculated. However, this would be computationally cumbersome. In the operational version of the ECMWF radiation code, $\overline{up}$ is simply the pressure-scaled absorber amount in the single layer $k$:

$$\overline{up} = \frac{1}{g} q_k \frac{p_k}{p_0} \Delta p_k. \tag{A.4}$$

This definition makes it possible to calculate the effective absorber amounts in a single loop from the top of the atmosphere to the surface (because it now follows that $u_e\,(p, p') = u_e(0, p') - u_e(0, p)$ for every $p$ and $p'$). However, the temperature correction factors are resolution-dependent: The better the resolution (the thinner the layers), the smaller the values of $\overline{up}$ become. In the theoretical limit of infinite resolution, $\overline{up} \to 0$, and the temperature correction would always be that for the case of weak absorption! It is this definition of $\overline{up}$ that was responsible for the slow convergence of the ECMWF longwave results.

In order to get rid of the convergence problem, we made the following ad-hoc modification:

$$\overline{up} = \frac{1}{g}\sum_{l=1}^{k} q_l \frac{p_l}{p_0} \Delta p_l. \tag{A.5}$$

Thus, the value of the pressure-scaled absorber amount integrated from the top of the atmosphere to the bottom of the layer $k$ is now assigned to $\overline{up}$. Whether this modification actually has a beneficial or detrimental effect on the temperature dependence of absorption, is uncertain, but the main point for this study is that the resolution dependence of the temperature correction factors is removed.

As an example of the effect of the modification, the longwave fluxes at the boundaries of the Midlatitude summer atmosphere with 300 ppmv of $CO_2$ are shown in Table 4 for both the original and modified versions of the code. Unlike the calculations reported elsewhere in this paper, $CH_4$ and $N_2O$ were not taken into account, so the case is identical to case 27 in Ellingson et al. (1991). The results are given for four grids: the LMD grid (11 layers), the ECMWF grid (31 layers), the reference grid (366 layers), and an extremely dense grid with 1688 layers. The results for "∞" layers were calculated in the last-mentioned grid so that

Table 4. *Clear-sky longwave fluxes ($Wm^{-2}$) at the boundaries of the mid-latitude summer atmosphere (test case 27 in Ellingson et al., 1991), calculated with the original and modified versions of the ECMWF radiation code in grids with different number of layers*

| | Downward flux at the surface | | | | | | |
|---|---|---|---|---|---|---|---|
| Layers | 11 | 31 | 366 | 1688 | "∞" | Ave | Std |
| original | 340.03 | 341.12 | 342.77 | 343.49 | 346.23 | 343.18 | 8.21 |
| modified | 339.07 | 339.63 | 339.82 | 339.84 | | | |
| | Upward flux at the top of the atmosphere | | | | | | |
| Layers | 11 | 31 | 366 | 1688 | "∞" | Ave | Std |
| original | 293.66 | 293.14 | 292.94 | 292.63 | 291.36 | 283.90 | 6.00 |
| modified | 293.77 | 293.44 | 293.66 | 293.67 | | | |

"Ave" and "Std" are the average value and the standard deviation of the results obtained in the ICRCCM comparison.

$\overline{up}$ was set to its limiting value zero. For comparison, the average value and the standard deviation of the results obtained in the ICRCCM project are also given.

The better convergence of the modified version of the code is clearly seen in the results; in particular the changes from 366 to 1688 layers are negligible. In grids with resolution typical to present atmospheric models, however, the differences between the two versions of the code are rather small (around 1 $Wm^{-2}$ in the downward flux at the surface and less than that in the upward flux at the TOA). For the Sub-Arctic winter atmosphere (not shown), the changes were considerably smaller. The changes in longwave cooling rates were typically of the order of 0.01 K/d, though they were somewhat larger in the few layers closest to the surface.

## REFERENCES

André, J. C. and Mahrt, L. 1982. The nocturnal surface inversion and influence of clear-air radiative cooling. *J. Atmos. Sci.* **39**, 864–878.

Betts, A. K., Ball, J. H. and Beljaars A. C. M. 1993. Comparison between the land surface response of the ECMWF model and the FIFE-1987 data. *Quart. J. Roy. Meteor. Soc.* **119**, 975–1001.

Carlson, M. A. and Stull, R. B. 1986. Subsidence in the nocturnal boundary layer. *J. Climate Appl. Meteor.* **25**, 1088–1099.

Clough, S. A., Iacono, M. J. and Moncet, J.-L. 1992. Line-by-line calculations of atmospheric fluxes and cooling rates: Application to water vapor. *J. Geophys. Res.* **97**, D14, 15761–15785.

Ellingson, R. G., Ellis, J. and Fels, S. 1991. The intercomparison of radiation codes used in climate models. Long wave results. *J. Geophys. Res.* **96**, D5, 8929–8953.

Fleagle, R. G. and Businger J. A. 1963. *An introduction to atmospheric physics.* Academic Press, New York, 346 pp.

Fouquart, Y. 1988. Radiative transfer in climate models. In: *Physically-based modelling and simulation of climate and climatic change. Part 1* (ed. M. E. Schlesinger). Kluwer Academic Publishers, Dordrecht, 223–283.

Fouquart, Y., Bonnel, B. and Ramaswamy, V. 1991. Intercomparing shortwave radiation codes for climate studies. *J. Geophys. Res.* **96**, D5, 8955–8968.

Funk, J. P. 1960. Measured radiative flux divergence near the ground at night. *Quart. J. Roy. Meteor. Soc.* **86**, 382–389.

Funk, J. P. 1962. Radiative flux divergence in radiation fog. *Quart. J. Roy. Meteor. Soc.* **88**, 233–249.

Garratt, J. R. 1994. Incoming shortwave fluxes at the surface. A comparison of GCM results with observations. *J. Climate* **7**, 72–80.

Geleyn, J.-F. 1981. Some diagnostics of the cloud/radiation interaction in ECMWF forecasting model. *ECMWF Workshop on Radiation and cloud-radiation interaction in numerical modelling, 15–17 October 1980*, 135–162.

Giorgetta, M. A. and Morcrette, J.-J. 1995. Voigt line approximation in the ECMWF radiation scheme. *Mon. Wea. Rev.* **123**, 3381–3383.

Hanson, H. P. and Derr, V. E. 1987. Parameterization of radiative flux profiles within layer clouds. *J. Climate Appl. Meteor.* **26**, 1511–1521.

Kondo, J. 1971. Effect of radiative heat transfer on profiles of wind, temperature and water vapor in the atmospheric boundary layer. *J. Meteor. Soc. Japan* **49**, 75–94.

McClatchey, R. A., Fenn, R. W., Selby, J. E. A., Volz, F. E. and Garing, J. S. 1971. *Optical properties of the atmosphere. AFCRL-71-0279*, Air Force Cambridge

Research Laboratories, Bedford, Massachusetts, 85 pp.

Morcrette, J.-J. 1989. Description of the radiation scheme in the ECMWF model. *Tech. Memo.* **165**, Res. Dep., ECMWF, Reading, 26 pp.

Morcrette, J.-J. 1991. Radiation and cloud radiative properties in the European Centre for Medium Range Weather Forecasts forecasting system. *J. Geophys. Res.* **96**, D5, 9121–9132.

Morcrette, J.-J. and Fouquart, Y. 1985. On systematic errors in parametrized calculations of longwave radiation transfer. *Quart. J. Roy. Meteor. Soc.* **111**, 691–708.

Morcrette, J.-J., Smith, L. and Fouquart, Y. 1986. Pressure and temperature dependence of the absorption in longwave radiation parameterizations. *Beitr. Phys. Atmos.* **59**, 455–469.

Olaguer, E. P., Yang, H. and Tung, K. K. 1992. A reexamination of the radiative balance of the stratosphere. *J. Atmos. Sci.* **49**, 1242–1263.

Ridgway, W. L., Harshvardhan and Arking, A. 1991. Computation of atmospheric cooling rates by exact and approximate methods. *J. Geophys. Res.* **96**, D5, 8969–8984.

Ritter, B. and Geleyn, J.-F. 1992. A comprehensive radiation scheme for numerical weather prediction models with potential applications in climate simulations. *Mon. Wea. Rev.* **120**, 303–325.

Rodgers, C. D. and Walshaw, C. D. 1966. The computation of infra-red cooling rate in planetary atmospheres. *Quart. J. Roy. Meteor. Soc.* **92**, 67–92.

Savijärvi, H. 1991. A model study of the PBL structure on Mars and the Earth. *Beitr. Phys. Atmos.* **64**, 219–229.

Shibata, K. and Uchiyama, A. 1994. An application of the discrete ordinate method to terrestrial radiation in climate models. *J. Atmos. Sci.* **51**, 3531–3538.

Smith, E. A. and Shi, L. 1992. Surface forcing of the infrared cooling profile over the Tibetan Plateau. Part I: Influence of relative longwave radiative heating at high altitude. *J. Atmos. Sci.* **49**, 805–822.

Stull, R. B. 1988. *An introduction to boundary layer meteorology.* Kluwer Academic Publishers, Dordrecht, 666 pp.